

photodiode (SM05PD1A, Thorlabs). The amplified photoacoustic or phosphorescence signals are acquired and saved along with the laser fluence signals by a data acquisition instrument (CS 14200, Gage Applied).

Nude mouse (Harlan, body weight ~ 20 g) ears were imaged to demonstrate the dual-modality microscopy of sO_2 and pO_2 *in vivo*. All experimental animal procedures were carried out in conformity with the laboratory animal protocol approved by the Animal Studies Committee of Washington University in St. Louis.

The PdT790 (10 mg/ml) was conjugated with bovine serum albumin (60 mg/ml) in 0.9% NaCl solution to provide a uniform environment for bound phosphors [5]. A 0.1 ml volume of the phosphorescent probe solution was bolus injected into the systemic vasculature via the tail vein. To allow the probe to equilibrate in the blood, image acquisition started 10 min after injection.

Photoacoustic images at wavelengths of 570 and 578 nm were captured. From the photoacoustic amplitude, aided by the molar absorption spectra of oxygenated hemoglobin (HbO_2) and deoxygenated hemoglobin (HbR), the relative concentrations of HbO_2 and HbR , and subsequently sO_2 , were calculated [1]. To measure the phosphorescence quenching, the phosphorescent light intensity was acquired for $500 \mu s$ at a sampling rate of 20 MHz. The relationship of pO_2 and the phosphorescence lifetime was assumed to follow the Stern–Volmer equation

$$\tau^{-1} = \tau_0^{-1} + k_q \cdot pO_2, \quad (1)$$

where τ_0 is the lifetime in the absence of O_2 and k_q is the quenching constant. The constants τ_0 and k_q have been experimentally calibrated and published in the literature [5,9]. We used the quenching constants for pH = 7.4 and temperature = $23^\circ C$ ($\tau_0 = 711 \mu s$, $k_q = 259 \text{ mmHg}^{-1} \text{ s}^{-1}$) [3]. A detailed description of the method used for computing sO_2 and pO_2 can be found in review articles [1,5].

To study the relationship of pO_2 and sO_2 *in vivo*, the blood pO_2 and pO_2 levels were modulated by switching the physiological state from systemic hyperoxia to normoxia in a mouse. Hyperoxia was induced by changing the inhalation gas to 100% O_2 , and the mouse was returned to normoxia by changing the inhalation gas to air. Prior to imaging, the mouse was exposed to each oxygen concentration for 10 min to stabilize the hyperoxic and normoxic states.

First, to explore the mapping of pO_2 and sO_2 , we imaged a nude mouse ear under hyperoxia. Figure 2(a) shows a photoacoustic image of the mouse ear vasculature acquired at 570 nm, an isosbestic wavelength where HbO_2 and HbR have identical molar absorption coefficients. Thus the photoacoustic amplitude measures the total hemoglobin (HbT) concentration. By combination with another photoacoustic image acquired at 578 nm, a pixel-by-pixel map of sO_2 was computed. As shown in Fig. 2(b), the arterioles and venules are visualized in pseudocolors of red and green, based on the different sO_2 levels. Figure 2(c) shows the time-integrated phosphorescence image, where sebaceous glands and blood vasculature can be seen as speckle and tree features, respectively. Autofluorescence from tissue often has a submicrosecond lifetime, while the phosphorescence

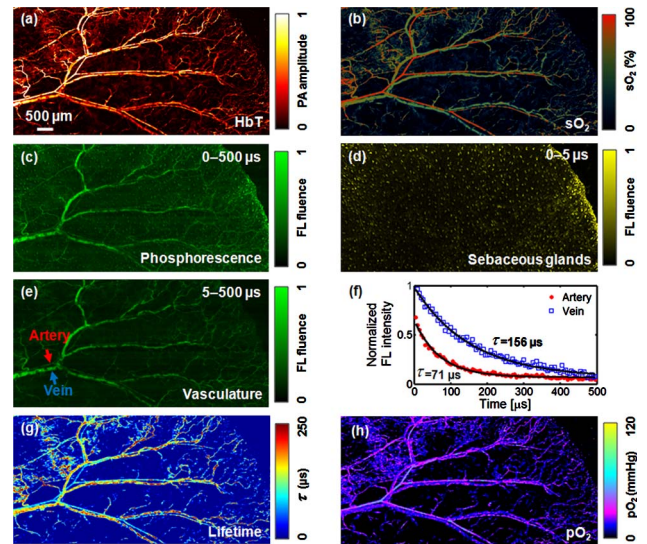


Fig. 2. (Color online) Imaging of the ear of a mouse in hyperoxia *in vivo*. (a) Photoacoustic image of total concentration of hemoglobin acquired at isosbestic 570 nm. (b) Photoacoustic image of sO_2 acquired at 570 and 578 nm. (c) Confocal image of time-integrated phosphorescence excited at 523 nm. Sebaceous glands and blood vessels are separated in the confocal images by integrating the phosphorescence signal (d) before and (e) after $5 \mu s$. (f) Phosphorescence decay curves from two regions of 15×15 pixels each in the artery and vein indicated by the arrows in (e). (g) Confocal image of the phosphorescence lifetime. (h) Confocal image of pO_2 : PA, photoacoustic; FL, fluorescence; HbT , total hemoglobin concentration; and τ , phosphorescence lifetime.

from the palladium porphyrin phosphorescent probe features $\sim 100 \mu s$ decay time. We split the phosphorescence signal at $5 \mu s$ so that the images of sebaceous glands [Fig. 2(d)] and blood vasculature [Fig. 2(e)] are separated. Figure 2(f) plots example of phosphorescence decay curves measured in the artery and vein labeled with arrows in Fig. 2(e). The phosphorescence lifetime was determined by fitting the measured data to an exponential decay curve ($R_2 = 0.98$ for arterial data and 0.99 for venous data). The shorter lifetime for the arterial data ($71 \mu s$) compared with that for the venous data ($156 \mu s$) shows phosphorescence quenching by dissolved blood oxygen. Pixelwise fitting produces a map of phosphorescence lifetime [Fig. 2(g)], which is further converted through Eq. (1) to a map of pO_2 [Fig. 2(h)]. A comparison of Figs. 2(b) and 2(h) shows that the blood vessels with higher sO_2 values measured by PAM have correspondingly higher pO_2 values measured by FCM, which agrees with known physiology [10].

To closely investigate the pO_2 and sO_2 levels in response to oxygen variation, sO_2 and pO_2 in hyperoxia (100% oxygen) and normoxia (21% oxygen) were mapped. We selectively analyzed an $\sim 1.5 \text{ mm} \times 1.5 \text{ mm}$ area of a mouse ear that contained four microvascular branching orders, as shown in Fig. 3(a) (photoacoustic image) and Fig. 3(b) (phosphorescence image). Figures 3(c)–3(f) show the sO_2 and pO_2 mappings for hyperoxic and normoxic conditions. Our results suggest that switching from hyperoxia to normoxia elicited a decrease in both sO_2 and pO_2 levels. They further suggest that in the artery, the sO_2 remained high ($>80\%$) while

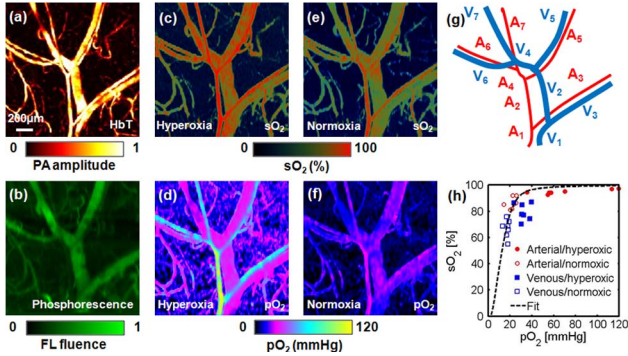


Fig. 3. (Color online) Photoacoustic and confocal microscopy of pO_2 and sO_2 levels in the ear of a mouse in response to switching from hyperoxia to normoxia. (a) Photoacoustic image of total concentration of hemoglobin acquired at 570 nm. (b) Confocal image of time-integrated phosphorescence in the same region excited at 523 nm. (c) Photoacoustic image of sO_2 and (d) confocal image of pO_2 in hyperoxia. (e) Photoacoustic image of sO_2 and (f) confocal image of pO_2 in normoxia. (g) Skeletons of arteries (A_i) and veins (V_i) shown in (a), where subscript i denotes the segmentation. (h) Plot of sO_2 versus pO_2 values in arteries and veins identified in (g). PA, photoacoustic; FL, fluorescence; and HbT, total hemoglobin concentration.

the pO_2 dropped significantly (from >100 mmHg to ~ 30 mmHg). In the vein, the decrease of sO_2 (from $\sim 80\%$ to $\sim 70\%$) was correlated with a smaller decrease in pO_2 (from ~ 35 mmHg to ~ 20 mmHg). Our observation is in agreement with the sigmoidal shape of the OHDC. The precapillary arteriolar and postcapillary venular trees are drawn in red and blue, respectively, in Fig. 3(g). The vasculature in the imaged region is segmented by different branching orders, and the sO_2 and pO_2 values were averaged within each segment (the correlation coefficient between sO_2 and pO_2 values = 0.62). We compared the experimental data with the classic OHDC equation developed by Kelman [11]

$$sO_2 = 100 \times \frac{a_1 + a_2x^2 + a_3x^3 + x^4}{a_4 + a_5x + a_6x^2 + a_7x^3 + x^4}, \quad (2)$$

where a_{1-7} are coefficients calibrated at the standard condition (temperature $T = 37^\circ\text{C}$, $\text{pH} = 7.4$, and CO_2 partial pressure $p\text{CO}_2 = 40$ mmHg), and

$$x = f(T, \text{pH}, p\text{CO}_2) \times pO_2, \quad (3)$$

$$f = 10^{[-0.024(T-37)+0.40(\text{pH}-7.40)-0.06(\log_{10}p\text{CO}_2-\log_{10}40)]}. \quad (4)$$

The conversion factor f alters the scale of the pO_2 axis in response to changes of temperature, pH, and CO_2 partial pressure [11]. Although both the blood pH and $p\text{CO}_2$ vary with the vasculature order and the physiological state [12], the OHDC maintains the sigmoidal shape. To demonstrate the nonlinear tendency for oxygen to bind to hemoglobin in the measured data, we applied a least-squares fitting of the pO_2 and sO_2 values to the above Kelman's equation with f being the fitting parameter. The fitted curve ($f = 1.83$) rises steeply with increasing pO_2 and reaches 90% sO_2 at pO_2 of 32 mmHg. The correlation coefficient between the fitted and measured sO_2 values was 0.67.

In summary, we developed an integrated PA-FCM system to image sO_2 and pO_2 as well as the total concentration of hemoglobin vessel by vessel *in vivo*. The ability to extract noninvasively sO_2 and pO_2 information in individual vessels makes the dual-modality microscope system a potential tool for quantitative analysis of oxygen transport and consumption in tissues.

We thank C. Zhang for helping with data processing and manuscript preparation. This work was sponsored in part by National Institutes of Health (NIH) grants R01 EB000712, R01 EB008085, R01 CA134539, U54 CA136398, and 5P60 DK02057933. L. Wang has a financial interest in Microphotoacoustics, Inc., and Endra, Inc., which, however, did not support this work.

References

1. S. Hu and L. V. Wang, *J. Biomed. Opt.* **15**, 011101 (2010).
2. D. Faber, E. Mik, M. Aalders, and T. van Leeuwen, *Opt. Lett.* **30**, 1015 (2005).
3. R. D. Shonat, E. S. Wachman, W. Niu, A. P. Koretsky, and D. L. Farkas, *Biophys. J.* **73**, 1223 (1997).
4. C. Zhang, K. Maslov, and L. Wang, *Opt. Lett.* **35**, 3195 (2010).
5. L.-W. Lo, C. J. Koch, and D. F. Wilson, *Anal. Biochem.* **236**, 153 (1996).
6. M. Yaseen, V. Srinivasan, S. Sakadzic, W. Wu, S. Ruvinskaya, S. Vinogradov, and D. Boas, *Opt. Express* **17**, 22341 (2009).
7. A. Estrada, A. Ponticorvo, T. Ford, and A. Dunn, *Opt. Lett.* **33**, 1038 (2008).
8. Y. Wang, K. Maslov, C. Kim, S. Hu, and L. V. Wang, *IEEE Trans. Biomed. Eng.* **57**, 2576 (2010).
9. M. Sinaasappel and C. Ince, *J. Appl. Physiol.* **81**, 2297 (1996).
10. G. S. Adair, *J. Biol. Chem.* **63**, 529 (1925).
11. G. R. Kelman, *J. Appl. Physiol.* **21**, 1375 (1966).
12. H. Kobayashi and N. Takizawa, *Am. J. Physiol. Heart Circ. Physiol.* **270**, 1453 (1996).